YMTHE, Volume *27*

Supplemental Information

ICOS Costimulation at the Tumor Site in Combination with CTLA-4 Blockade Therapy Elicits Strong Tumor Immunity

Mario Martínez Soldevilla, Helena Villanueva, Daniel Meraviglia-Crivelli, Ashwathi Puravankara Menon, Marta Ruiz, Javier Cebollero, María Villalba, Beatriz Moreno, Teresa Lozano, Diana Llopiz, Álvaro Pejenaute, Pablo Sarobe, and Fernando Pastor

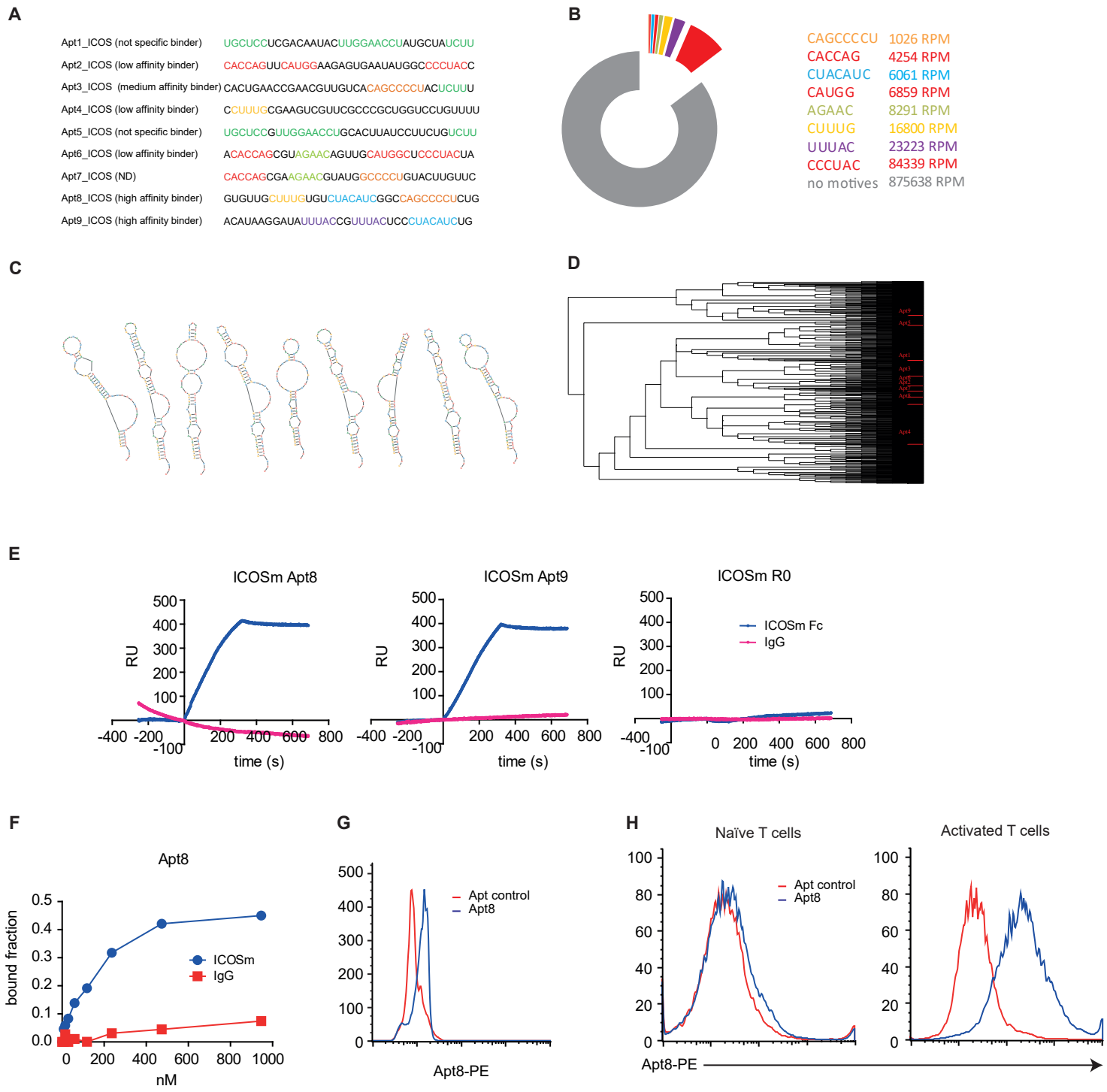

Fig.S1. Selection and in vitro characterization of ICOS-binding aptamers. A) Most abundant aptamer species identified after round 6 of SELEX by Ion Torrent sequencing against ICOS recombinant protein. The constant regions from the 5′ end (5′GGGGAATTCTAATACGACT-CACTATAGGGAGAGATAGTGTAGGG-3′) and from the 3′ end (5′-CCCTCACTCCTCTCCCTCC-3’), have been removed for carity. Sequence similarities among aptamers of the same family are shown in different colors. B) Frequencies of the most conserved RNA moieties after round 6 depicted in different colors. C) Secondary structure of the nine most abundant aptamers predicted by using RNAstructure software. D) The sequences of aptamer identified from round 6 were HT-sequenced and alignment was conducted with FASTAptamer and clustered by ClustalW. E) Binding of Apt8 and Apt9 to murine chimera recombinant protein ICOSm-Fc (blue) and as control protein IgG (red) detected through Surface Plasmon Resonance (SPR) at 50 nM concentration of proteins. R0 randomized library was used as negative control. F) Nitrocellulose filter binding assay of Apt8 to the recombinant mICOS-Fc (blue) and to IgG (red) at different concentrations to assess the aptamer’s binding affinity. E) Apt8 binding to ICOS-Fc coated beads measured by flow cytometry. H) Apt8-PE binding (blue) to naïve (ICOS-null cells) or activated T lymphocytes (ICOS-expressing cells), determined by flow cytometry.

A

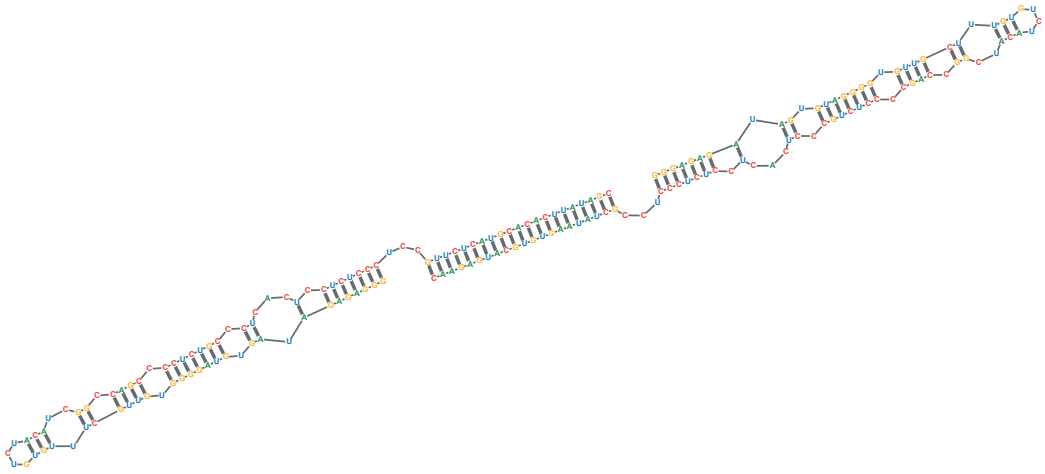

B

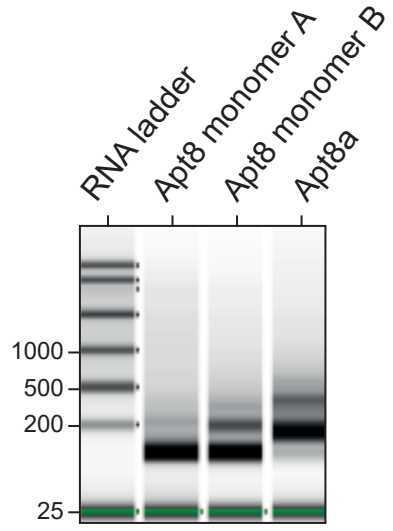

Fig. S2. Structure of Apt8 dimer (Apt8a). A) Predicted secondary structure of Apt8a generated by hibridization of two complementary sequences (monomer A and B) added at the 3' end of the aptamer. B) Separation of Apt8a by PAGE.

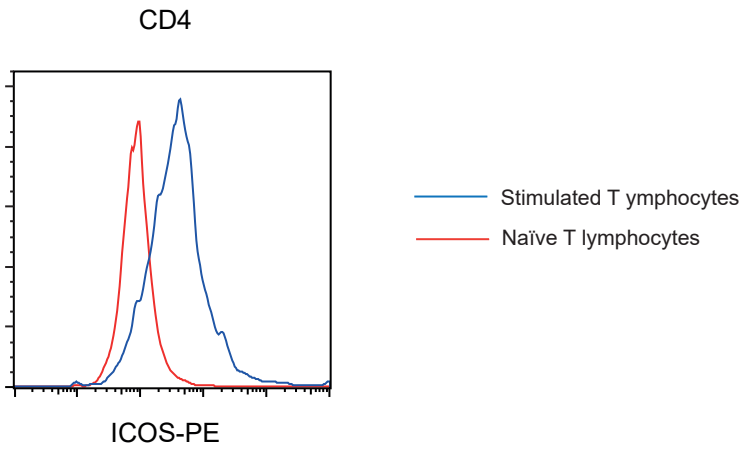

Fig. S3. Induction of ICOS expression on $CD4^+$ lymphocytes after CD3 stimulus.

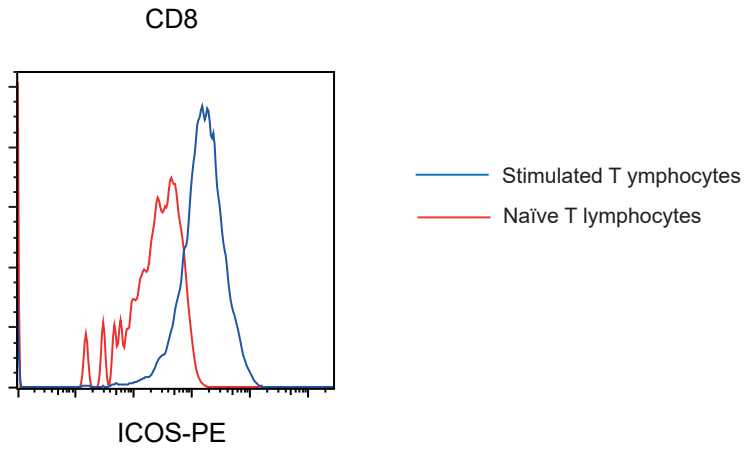

Fig. S4. Induction of ICOS expression on OT-I CD8^{+} lymphocytes after stimulus.

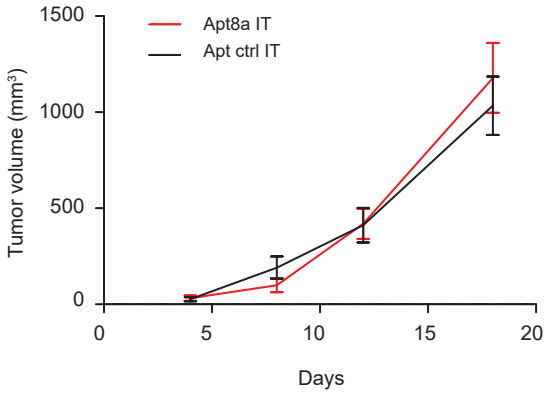

Fig. S5. Tumor kinetics of B16/F10 tumor bearing mice with Apt8a monotherapy. Mice treated intratumorally (IT) with Apt8a as monotherapy or with Apt-ctrl following the schedule depicted in Figure 2A (n=6).

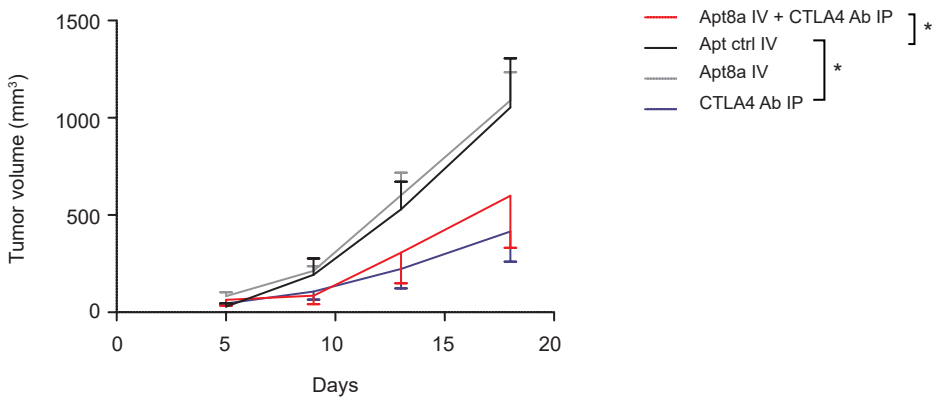

Fig. S6. Tumor kinetics of B16/F10 tumor bearing mice with Apt8a intraveneously. Mice treated systemically with Apt8a intravenously (IV) and anti CTLA4 antibody (9H10) intraperitoneally (IP) following the schedule depicted in Figure 2A (n=5).

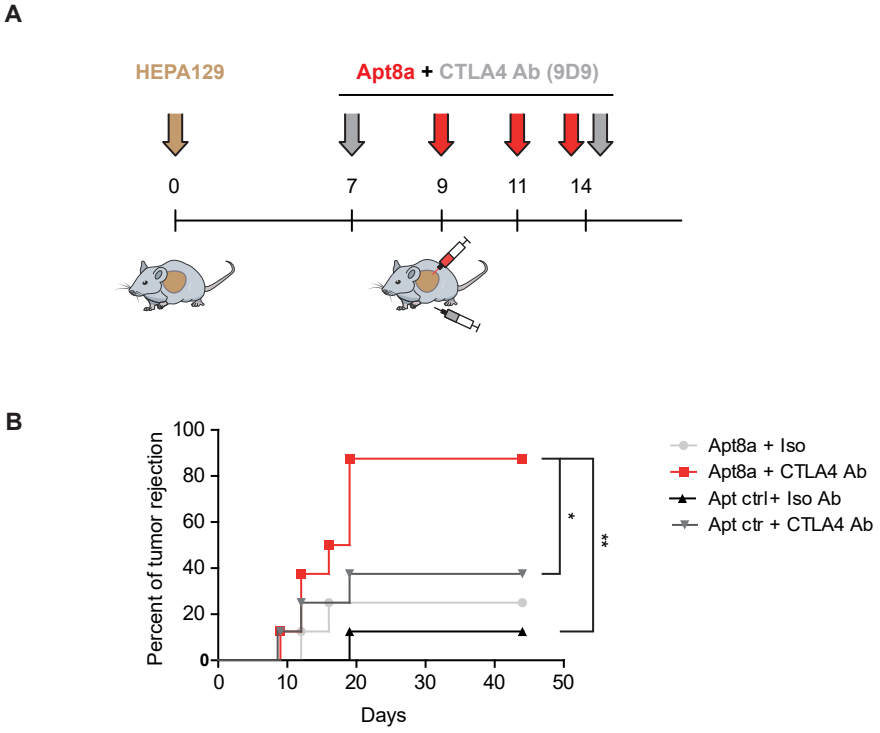

Fig. S7. Intratumoral ICOS agonist (Apt8a) potentiates CTLA-4 blockade therapy in a hepatocarcinoma mouse model. A) HEPA hepatocarcinoma was implanted subcutaneously in C3H mice. On days 7 and 14, mice were injected intraperitonealy with CTLA-4 blocking antibody (9D9) and intratumorally with Apt8a or Apt ctrl at day 9, 10 and 14. B) Percentage of tumor rejection in the treated mice is depicted (n=8 per group).

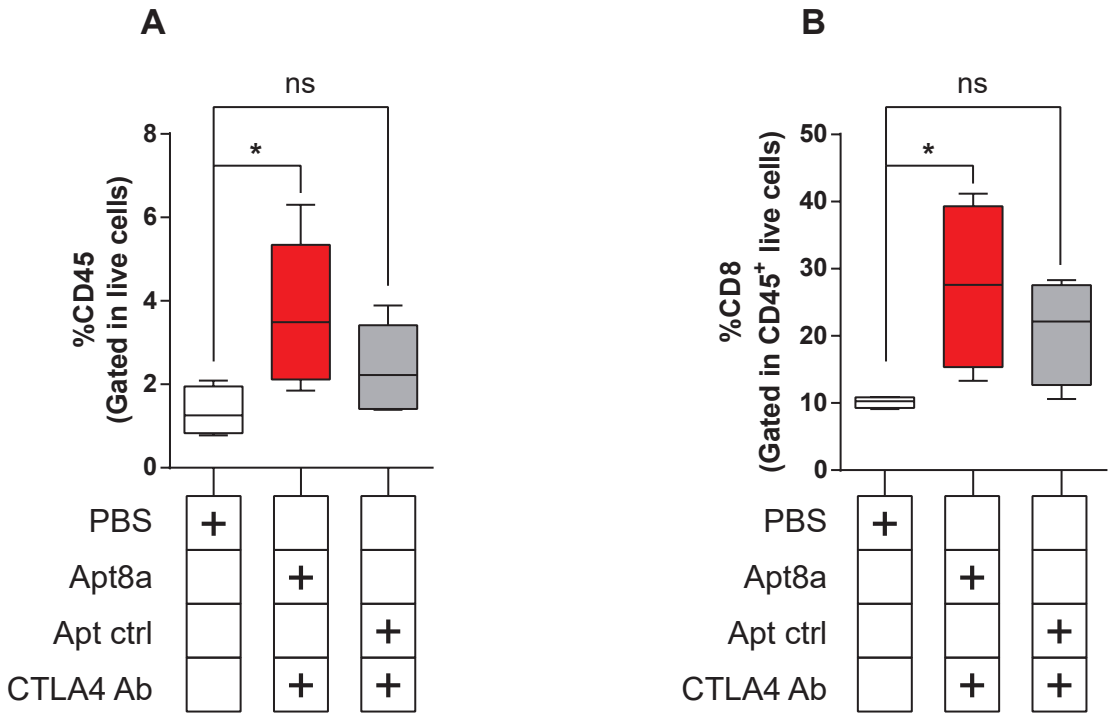

Fig. S8. Effect on the immune cell infiltration of Apt8a intratumoral injection with anti CTLA-4 antibody therapy. B16/F10 tumor bearing mice were treated as depicted in Fig. 2A at day 14 mice were sacrified and tumor was procesed to staint with anti CD8 (A) and anti CD45 (B) antibodies. The samples were adquired and analised by flow cytometry. (n=4 mice)

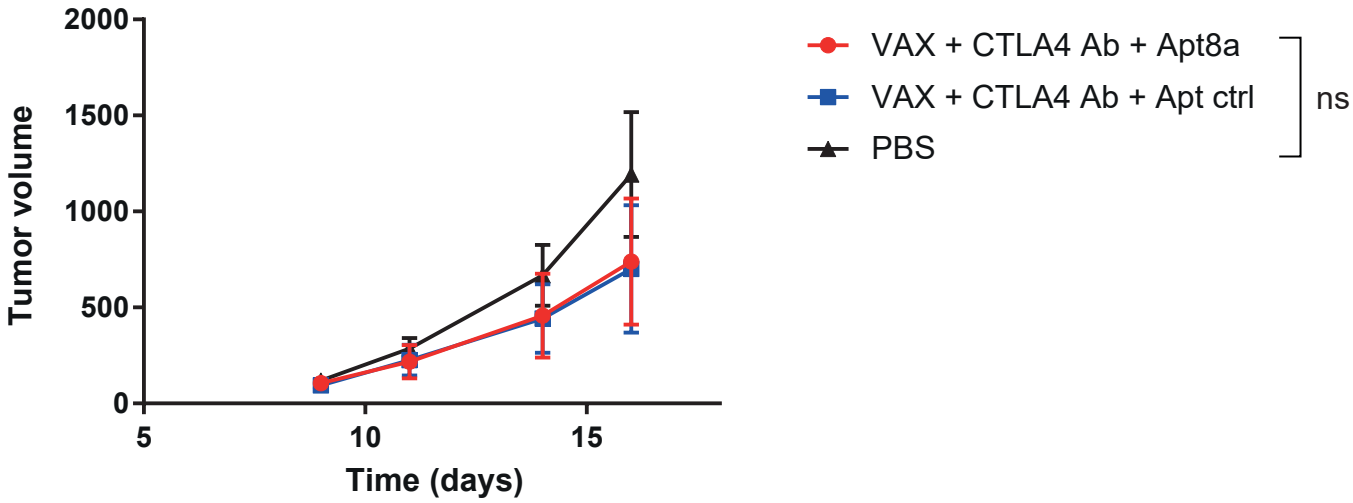

Fig. S9. Tumor kinetics of B16-MRP1 tumor bearing mice treated with VAX (irradiated tumor cells), anti CTLA-4 antibody and intravenous Apt8a following the same schedule depicted in figure 5C. (n=6).

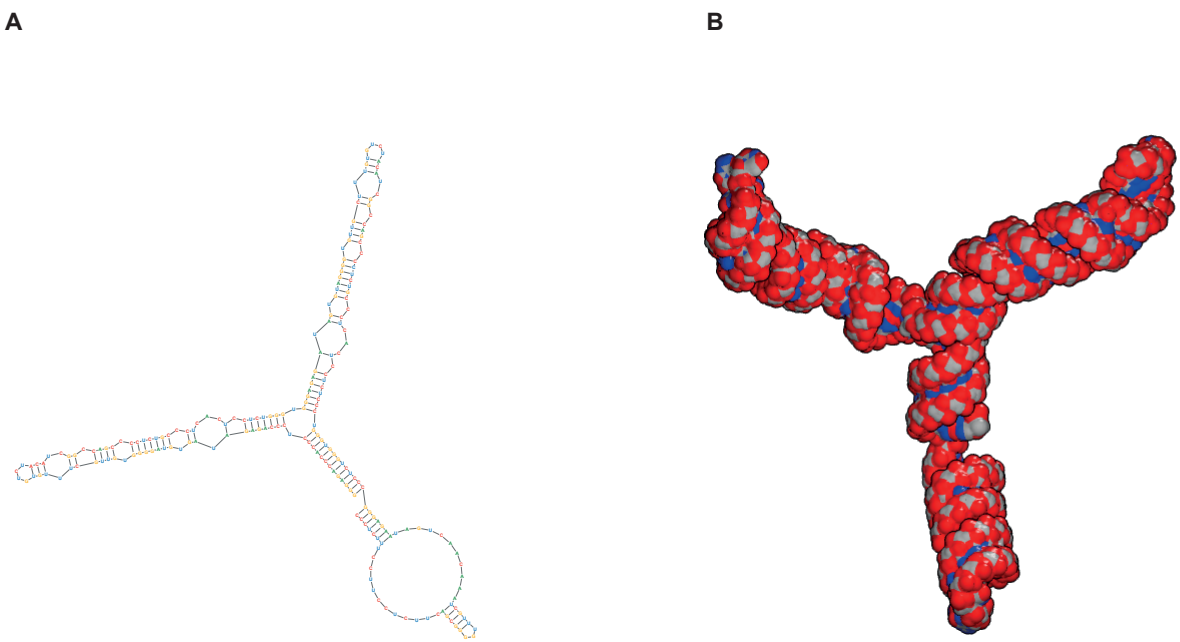

Fig. S10. MRP1-ICOS aptamer structure. A) Predicted secondary structure of MRP1-ICOS aptamer using RNAstructruture software. B) Predicted tertiary structure of MRP1-ICOs aptamer by Rosseta software.

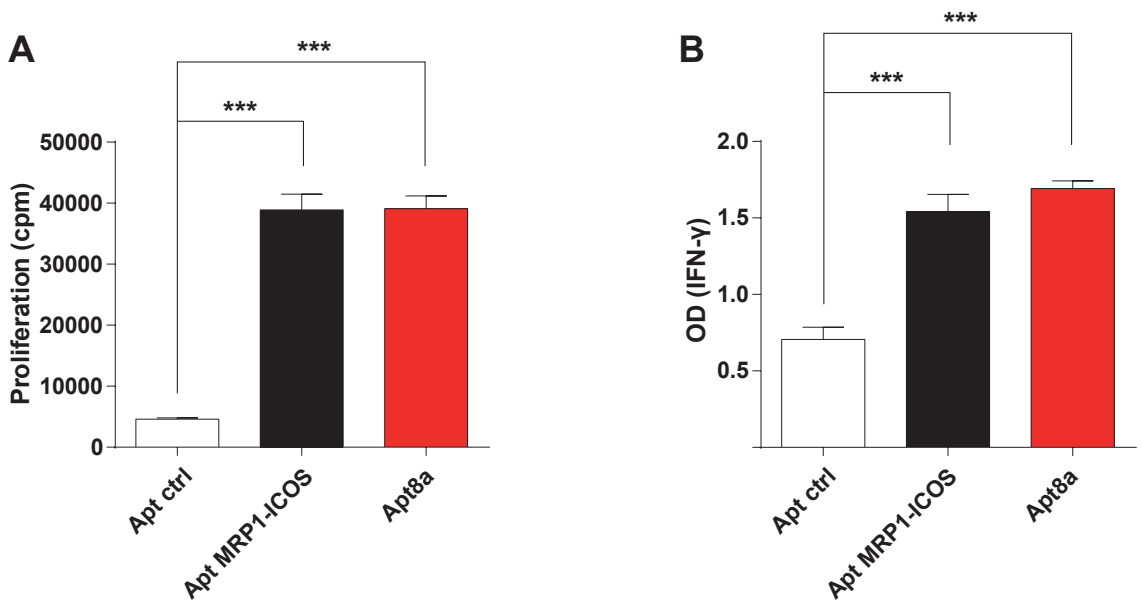

Fig. S11. Magnitude of Atp8a and Apt MRP-ICOS costimulation. CD8 lymphocytes suboptimally activated with anti-CD3 agonistic antibody where costimulated with 0.5μM of Apt8a (red) or Apt MRP1-ICOS (black). 72 hours later proliferation was determined by ^{3}H incorporation (A) by IFN-γ secretion measured by ELISA (B).

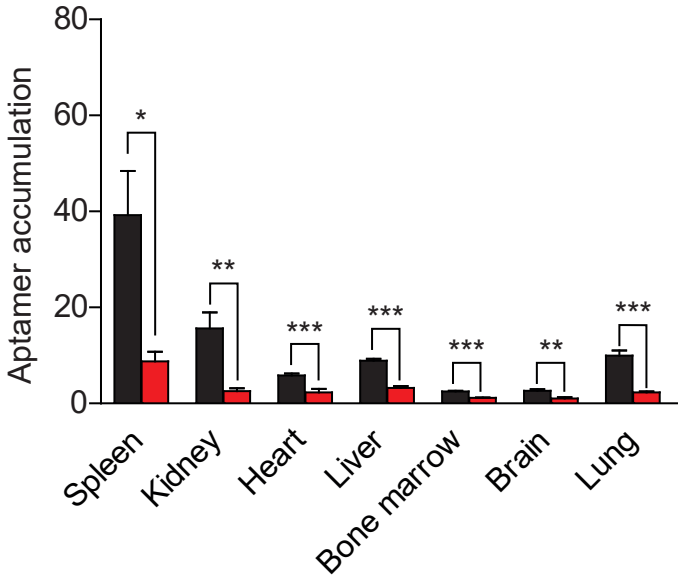

Fig. S12. Biodistribution of MRP1-ICOS aptamer and Apt8a in mice after intravenous injection. Apt8a treated mice in black and MRP1-ICOS bi-specific aptamer treated mice in red. Aptamers were detected by qRT-PCR using specific primers (Sel-Fwd and Sel-Rev) described in supplementary methods and normalized to the constitutive endogenous gene (HPRT).

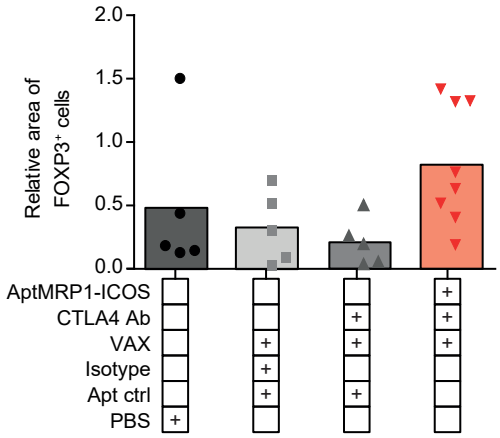

Fig. S13. Effect of MRP1-ICOS bi-specific aptamer combination treatment on FOXP3$^+$ cells. FOXP3$^+$positive cells measured by immunofluorescence in the tumors of treated mice as in Figure 7A.

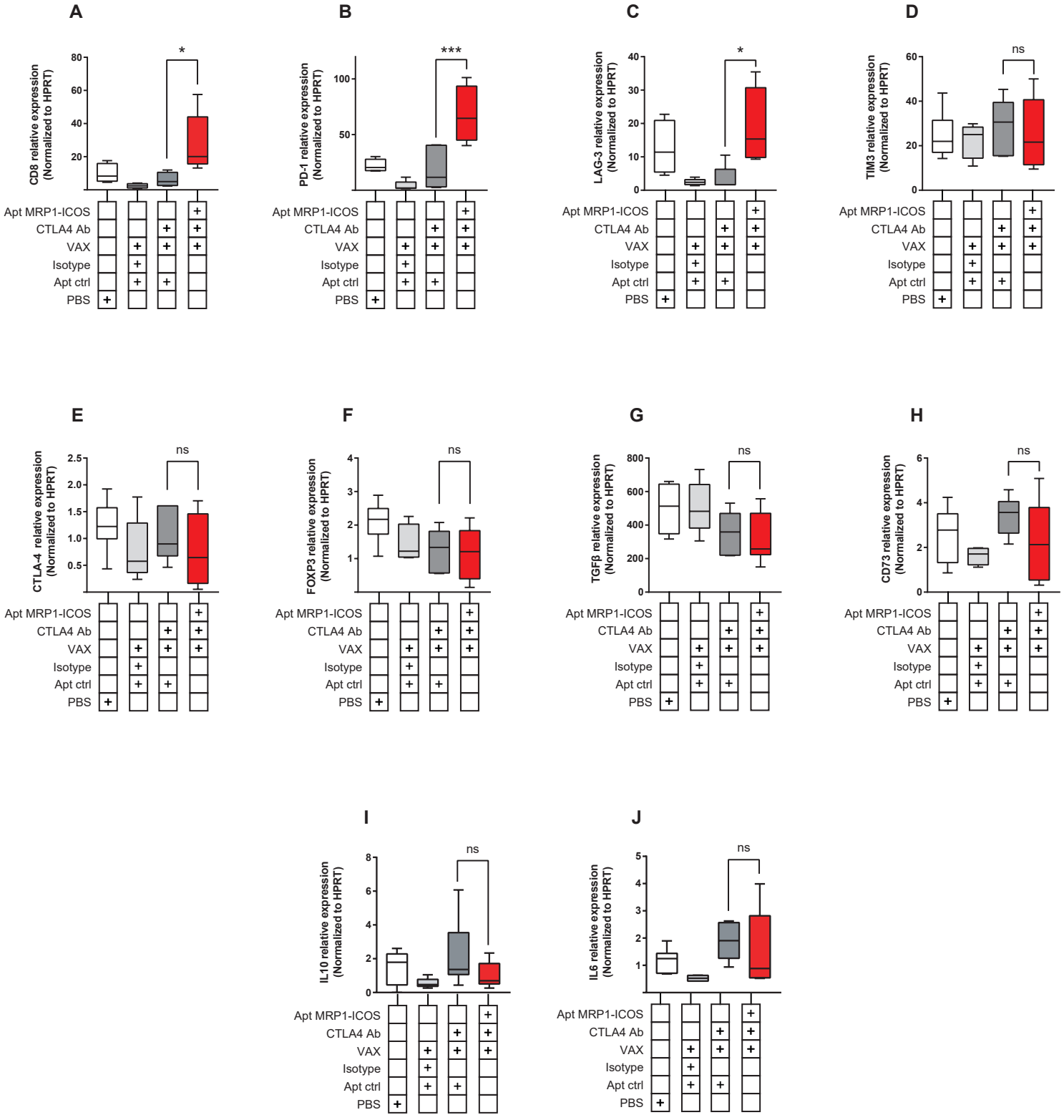

Fig. S14. Effect of MRP1-ICOS bi-specific aptamer combination treatmenton the tumor gene immune profile. B16-MRP1 mice receiving the treatment depicted in Fig. 5C were analyzed by qRT-PCR for the expression of CD8 (A), PD-1(B), LAG-3 (C), TIM-3 (D), CTLA-4 (E), FOXP3 (F), TGF-β (G), CD73 (H), IL10 (I) and IL6 (J).

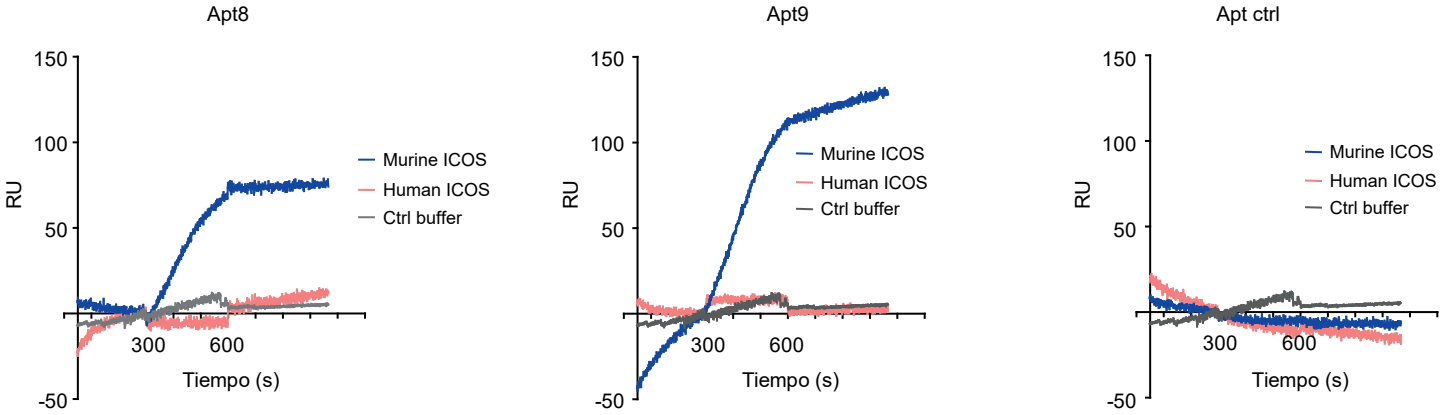

Fig.S15. Binding of Apt8 and Apt9 to mouse and human ICOS proteins measured by SPR.

Table S1. SELEX conditions

Round	**RNA (μM)**	**ICOS-Fc (nM)**
1	2	1
2	1	0.5
3	0.25	0.5
4	0.125	0.5
5	0.015	0.5
6	0.015	0.3

Supplementary material

ICOS aptamer selection by HT-SELEX

Anti-ICOS RNA aptamers were selected through high-throughput sequencing SELEX using a recombinant Fc tagged ICOS protein as target after counter selection with an Fc tagged control protein. RNA Transcription used to generate selection libraries was performed with 2' fluoropyrimidines to increase RNA stability and resistance to RNAses. The selection was conducted at increasingly restrictive conditions to favor the selection of aptamers with higher affinities to target after every round of SELEX (Table S1). The selection was stopped at round 6 as we observed that the RNA recovery was reaching a plateau. Rounds 5 and 6 RNA aptamer libraries were high-throughput sequenced by Ion Torrent. The sequence aptamer analysis was carried out using Galaxy and FASTAptamer softwares. We selected the nine most prevalent aptamers in round 6 for further analysis and characterization (Fig. S1A). The enriched selected aptamers were further analyzed for clusterization by using ClustalW software. The phylogenetic distribution of all the aptamer families at round 6 is shown in Fig. S1D.

Binding affinities of the most abundant aptamer families were assessed by ^{32}P blotting. We observed that some higher affinity aptamers such as Apt1 and Apt5 were not specific to the target molecule, ICOS, as they could also bind other recombinant proteins. Aptamers 2, 4 and 6 were low affinity binders with Kds greater than 200 nM . Apt8 and Apt9 were high affinity binders, with Kds determined to be less than 50 nM. Interestingly, Apt8 had one of the highest affinities even though it showed accumulation of RNA motif sequences that were also shared by low affinity binders. These results support our previous observation that aptamer species with higher affinity contain binding domains present in other lower affinity aptamers (CMA) (Soldevilla et al, PlosOne 2017), putting into perspective that selection generates aptamers that likely display multiple accumulative binding sites and the sum of their ability to bind target is what determines their final augmented affinity. Probably the most important binding moieties formed within the aptamer sequences are CUACAUC and CAGCCCCU. The proportion of all potential binding site sequences (CAGCCCCU, CUACAUC, CACCAG, CAUGG, AGAAC, CUUUG, UUUAC, CCCUAC) are shown in Fig. S1B. The secondary structure of each aptamer was predicted by using RNAStructure software (Fig. S1C); conserved motifs that might be relevant in binding to ICOS protein are depicted and annotated in color. Binding of Apt8 and Apt9 was also confirmed by surface plasmon resonance (SPR) (Fig. S1E). We also wanted to test whether the aptamers were able to recognize the human ICOS protein that has high homology with the murine one. No binding to human ICOS-Fc was detected by SPR reflecting the high specificity of these aptamers (Fig. S15).

Apt8 was selected to carry out all further experiments as it was given higher yiels of in vitro production reducing cost for in vivo experiment where higher amount material is require, nonetheless Apt9 could be engineered for a potential ICOS agonist. We further validated binding of Apt8 by flow cytometry to beads coated with ICOS protein (Fig. S1G), and to cells expressing ICOS (Fig. S1H). To that end, we used activated CD4+ lymphocytes on which ICOS is induced, and naïve T cells as negative controls (Fig. S3).

Supplementary Methods and Materials

Aptamer HT-SELEX

SELEX was performed as previously described against a chimeric-recombinant ICOS-IgG protein that comprises of the extracellular domain of mouse ICOS fused to human IgG1-Fc (R&D, Minneapolis, MN, USA. Ref:168-CS-100). A 31N-nucleotide randomized DNA library flanked by two constant regions was used the template library for selection: GGAGGGAGAGGAGTGAGGGNNNNNNNNNNNNNNNNNNNNNNNNNNNNNNNNNNNCCCTACACTATCTCTCCC; the primers used for library amplification were: Fwd-Sel GGGGAATTCTAATACGACTCACTATAGGGAGAGATAGTGTAGGG and Rev-Sel GGAGGGAGAGGAGTGAGGG. 2-Fluoro-UTP and 2-Fluoro-CTP modification was included during RNA transcription to improve RNA stability and increase resistance to RNAses. All in vitro transcriptions were performed with the DuraScribe kit (Epicentre, Madison, WI, USA). In Table, S1 selection conditions for each round of SELEX are described. The binding of the library to the target protein was carried out at 37°C in saline buffer (20mM HEPES, 150 mM NaCL, 2mM CaCl2 and 0.01% BSA) for 30 minutes. mICOS-Fc recombinant protein was immobilized to protein A bound sepharose beads (GE Healthcare Bio-science, Uppsala, Sweden). The RNA-bound fraction was extracted via phenol-chloroform-isoamyl alcohol fractionation; the recovered RNA was precipitated. Eluted RNA was retro-transcribed and amplified by PCR, as previously described. In each round of SELEX, we performed counter-selection against human IgG1 bound to sepharose beads (Sigma Aldrich, Saint Louis, MO).

The aptamer libraries generated after round 5 and 6 were HT-sequenced by Ion Torrent, and analysis of multiple-sequence alignment was performed by using FASTAptamer software. The results from FASTAptamer were clustered with ClustalW and visualized with Seaview software. All the processes were conducted in a Linux CentOS 6.3 cluster of 4 cores and 64GB. RNA-structure predictions were performed with RNAstructure 5.3 software.

All selected aptamers were directly generated from transcriptions of double-stranded DNA oligonucleotide templates which were hybridized from two partially complementary sequences and extended by Klenow reaction. The purified DNA template was transcribed using the T7 DuraScribe Kit and purified by polyacrylamide gel electrophoresis (PAGE).

Dimeric aptamers were produced by engineering the 3′ end of each aptamer to create two complementary regions so they could be attached together by hybridization. After annealing, dimeric aptamers were purified by PAGE and concentrated using a 30 kDa Amicon® Ultra-4 column in PBS.

The MRP1-ICOS bi-specific aptamer was engineered to include MRP1 binding aptamer and the costimulatory ICOS Apt8a, resulting in the following sequence; 5' - GGGGAATTCTAATACGACTCACTATAGGGAGACCCACCCTCCCAGAGATAGTGTAGGGGTGTTGCTTTGTGTCT ACATCGGCCAGCCCCTCTGCCCTCACTCCTCTGGGTGGGAGAGATAGTGTAGGGGTGTTGCTTTGTGTCTACAT CGGCCAGCCCCTCTGCCCTCACTCCTCTCCCTGGGTGGGTCTCCCGGGAGAATAGTCAACAAATCGTTTGGGGC GACTTCTCCTTCCTTTCTCCC-3'. It was further cloned into the pUC57 plasmid. This product was used as template for the PCR with the following primers: Fwd-bi 5′-GGGGAATTCTAATACGACTCACTATAGGG-3′ and Rev-bi 5′-GGGAGAAAGGAAGGAGAAGTC-3′. The PCR product was purified and *in vitro* transcribed with Durascribe.

SPR

Aptamer binding to ICOS protein was determined by surface plasmon resonance using the ProteOn XPR36 system. Biotinylated aptamers were immobilized onto independent channels of streptavidin coated sensor chips (Bio-Rad). ICOS-Fc or control Fc protein was injected in a 50 nM running buffer consisting of PBS and 0.005% [v/v] Tween 20, pH 7.4 at a flow rate of 30 µl/min.

Binding to beads

mICOS recombinant protein (R&D, Minneapolis, MN, USA. Ref:168-CS-100) was conjugated to Dynabeads® M-450 Tosylactivated (Invitrogen, Life technologies, Carlsbad, CA, USA. Ref: 14013) following manufacturer's instructions. ICOS-beads were stained with 50 pmol of the biotinylated aptamer and 0.05 µg/µl of streptavidin-PE for 30 minutes at 37 °C. Afterwards, cells were washed twice with PBS (Gibco, Life Technologies, Waltham, MA, USA. Ref: 14190-094) and analyzed by flow cytometry (BD Bioscience, San Diego, CA, USA) and analyzed using FlowJo vX.0.7.

Assessment of ICOS expression in T lymphocytes

10^5 CD4 were isolated from spleen by Mylteny keit and were activated for 24 hours with 1 µg/ml of anti-mouse CD3e coated on a 96 well plate (BD Biosciences, San José, CA, USA. Ref: 145-2C11) and SIINFEKL (GeneCust, Ellange, Luxembourg. Ref: PO#P160373_2). 10^5 CD8 OT-I isolated lymphocytes were activated with 1 µg/ml of SIINFEL for 24 hours. CD4 lymphocytes were , washed with PBS buffer and stained with either CD4 PE clone GK1.5 at dilution 1:200 and ICOS APC clone C398.4A at dilution 1:400. CD8 OT-I lymphocytes were stained withCD8 APC clone 53.67 at dilution 1:400 and ICOS PE clone 15F9 at dilution 1:400, (BioLegend, San Diego, CA, USA. Ref: 100407, 313509, 100712 and 107705 respectively)

for 20 minutes at 4ºC. Cells were washed twice with PBS buffer and analyzed by flow cytometry using the BD FACSCalibur™ (BD Bioscience, San Diego, CA, USA) and analyzed using FlowJo vX.0.7.

Binding to cells measured by flow cytometry

10^5 $CD4^+$ cells were activated with anti-mouse CD3e, washed with PBS buffer and stained with 50 pmol of the biotin-Apt8 and 0.05 μg/μl of streptavidin-PE for 30 minutes at 37ºC. Naïve T lymphocytes were stained as well as negative control. Afterwards, cells were washed twice with PBS buffer and analyzed by flow cytometry using the BD FACSCalibur™ and analyzed using FlowJo vX.0.7.

3D-Structure prediction

For each modeled aptamer, the most stable 2D structure was generated by using RNAstructure 5.3. For the generation of 3D RNA structures, the Rosetta package FARFAR was used to build a total of 200 models. Next, the models were sorted by Rosetta energy and selected for 3D structural clustering with an auto-adjusted radius. After examining the cluster population distribution, the lowest Rosetta energy representative model was selected from the most populated cluster for further visual inspection.

qRT-PCR for immune gene profile in tumor samples

RNA from the tumor tissue was extracted with TRIzol (Life Technologies, Carlsbad, CA, USA). 2 μg of RNA was retrotranscribed (Applied Biosystems, Foster city, CA, USA). and amplified by quantitative PCR in 790047 Fast Real Time PCR machine with SYBR green using the following primers: TIM3-FWD AGACATCAAAGCAGCCAAGGT, TIM3-REV TCCGTGGTTAGGGTTCTTGG, LAG3-FWD CTTCACCTTGAGGCTGTGGG, LAG3-REV GGAGTCACTGTGATGACCGC, CTLA4-FWD AGGTGGAACTCATGTACCCAC, CTLA4-REV AGGAAGTCAGAATCCGGGCA, IL6-FWD AGCCAGAGTCCTTCAGAGAGAT, IL6-REV AGGAGAGCATTGGAAATTGGGG, IL10-FWD AGGCGCTGTCATCGATTTCT, IL10-REV ATGGCCTTGTAGACACCTTGG, PD1-FWD GGAGACTGCTACTGAAGGCG, PD1-REV CCCTGATTGCCAGCTCAACT, CD73-FWD GGACATTTGACCTCGTCCAAT, CD73-REV GGGCACTCGACACTTGGTG, CD8-FWD CCGTTGACCCGCTTTCTGT, CD8-REV CGGCGTCCATTTTCTTTGGAA, TGFB-FWD GGATACCAACTATTGCTTCAGCTCC, TGFB-REV AGGCTCCAAATATAGGGGCAGGGTC, FOXP3-

FWD CACCTATGCCACCCTTATCCG, FOXP3-REV CATGCGAGTAAACCAATGGTAGA. All the primer sets have been validated by sequencing each amplicon by Sanger.

Cells and Media

B16/F10 melanoma cells were obtained from ATCC and cultured with DMEM medium (Gibco, Life Technologies, Waltham, MA, USA. Ref: 41966-029) supplemented with FBS 10% (Merck, Darmstadt, Germany. Ref: S0115), L-Glutamine 1% (Gibco, Life Technologies, Waltham, MA, USA. Ref: 25030024) and P/S 1% (Gibco, Life Technologies, Waltham, MA, USA. Ref: 15140-122). B16-MRP1 melanoma cells were obtained as described before (Soldevilla MM Oncotarget 2016) and cultured with DMEM medium (Gibco, Waltham, MA, USA. Ref: 41966-029) supplemented with FBS 10% (Merck, Darmstadt, Germany. Ref: S0115), L-Glutamine 1% (Gibco, Life Technologies, Waltham, MA, USA. Ref: 25030024) and P/S 1% (Gibco, Life Technologies, Waltham, MA, USA. Ref: 15140-122). Hepa129 were obtained from ATCC and cultured with RPMI 1640 (Gibco, Life Technologies, Waltham, MA, USA. Ref: 42401-018) supplemented with FBS 10% (Merck, Darmstadt, Germany. Ref: S0115) and P/S 1% (Gibco, Life Technologies, Waltham, MA, USA. Ref: 15140-122).

Lymphocyte medium was obtained adding the following supplements to RPMI 1640 medium (Gibco, Waltham, MA, USA. Ref: 42401-018); β-mercaptoetanol 50μM (Sigma-Aldrich, Merck, Darmstadt, Germany. Ref: M-6250), FBS 10% (Merck, Darmstadt, Germany. Ref: S0115), L-Glutamine 1% (Gibco, Life Technologies, Waltham, MA, USA. Ref: 25030024), NEAA 1% (Gibco, Life Technologies, Waltham, MA, USA. Ref: 11140-035), NaPyruvate 1% (Gibco, Life Technologies, Waltham, MA, USA. Ref: 11360-039), HEPES 1% (Gibco, Life Technologies, Waltham, MA, USA. Ref: 15630-056) and P/S 1% (Gibco, Waltham, MA, USA. Ref: 15140-122). PBS buffer was obtained by adding 0,5% BSA (Sigma-Aldrich, Merck, Darmstadt, Germany. Ref: A9647-100G) and 2mM EDTA (Invitrogen, Life Technologies, Waltham, MA, USA. Ref: 15575-038) to PBS without $MgCl_2$ nor $CaCl_2$.

Hepa 129 hepatocarcinoma

10^6 Hepa 129 hepatocarcinoma cells were implanted in the right flank of 6-8 week-old female C3H mice. At days 7 and 14 post tumor inoculation, 50 μg of anti-mouse CTLA-4 clone 9D9 or isotype antibody (BioXCell, West Lebanon, NH, USA) was administered intraperitonially. At days 9, 11 and 14 post tumor injection, 250 pmol of Apt8a or Apt-ctrl was administered intratumorally. Mice were allocated into 4 groups; Isotype, Isotype + Aptamer, anti-CTLA-4 + Apt-ctrl and

anti-CTLA-4 + Apt8a. The antitumor effect elicited by these treatments was measured by evaluating the percentage of tumor-free mice by determining the absence of tumor after the treatment.